Transportation Geotechnics 30 (2021) 100617

Contents lists available at ScienceDirect

Transportation Geotechnics

journal homepage: www.elsevier.com/locate/trgeo

Mechanical response of full-scale geosynthetic-reinforced asphalt overlays subjected to repeated loads

V. Vinay Kumar [a,*], Sireesh Saride [b], Jorge G. Zornberg [a]

[a] Department of Civil, Architectural and Environmental Engineering, University of Texas at Austin, Austin, TX 78712, USA
[b] Department of Civil Engineering, Indian Institute of Technology Hyderabad, Telangana 502285, India

ARTICLE INFO

Keywords:
Geosynthetics
Asphalt overlay
Full-scale instrumented pavement model
Cumulative permanent deflection
Traffic benefit ratio
Rut depth reduction

ABSTRACT

This study aims at evaluating the influence of geosynthetic reinforcements on the structural improvement of asphalt overlays placed on distressed pavement layers using repeated load tests. Full-scale instrumented pavement models were constructed in an indoor steel tank measuring 1000 mm in length, 1000 mm in width and 1000 mm in depth. Full-scale instrumented pavement models consisted of a 650-mm-thick weak subgrade, 250-mm-thick base, 90-mm-thick distressed asphalt layer, binder tack coat, geosynthetic reinforcement (except in control sections), and 50-mm-thick hot mix asphalt overlay. Sensors used in the instrumentation program included earth pressure cells and linear variable displacement transformers installed on the subgrade and surface layers, respectively. Four different geosynthetic types, including woven geo-jute mat (GJ), polypropylene geogrid (PP), polyester geogrid (PET), and fiberglass geogrid composite (FGC) were adopted as asphalt reinforcements. A servo-hydraulic actuator was used to replicate a live traffic wheel load by applying an equivalent single axle contact pressure of 550 kPa at a frequency of 1 Hz. Repeated load tests were terminated after 100,000 load cycles and the behaviour of geosynthetic-reinforced full-scale models was compared with that of unreinforced model. Performance indicators, including Traffic Benefit Ratio (TBR) and Rut Depth Reductions (RDR), were estimated and repeated load test results indicated an increase in the structural performance of geosynthetic-reinforced full-scale models in relation to that of unreinforced model. Among the geosynthetic-reinforced models considered in this study, the FGC-reinforced model showed a comparatively better performance with a maximum TBR of 20 at a permanent deflection of 5 mm and the highest RDR of 56% after 100,000 load cycles, respectively. Maximum reductions of 56% in surface deflection and of 30% in vertical pressure on the subgrade were also observed after 100,000 load cycles in the FGC-reinforced model.

Introduction and background

A conventional rehabilitation program adopted to restore the serviceability and skid resistance of distressed asphalt and cement concrete pavements involves the construction of a structural asphalt overlay, the thickness of which should be optimized. Such optimization results from balancing the excessive raw material costs that would result if a thick asphalt overlay is adopted with the inadequate performance (e.g. due to early reflective cracks) that would occur if a thin overlay is constructed. Reflective cracks are discontinuities and cracks in the new overlays that have propagated from the old/existing pavement surface under traffic and temperature loads [8,22]. Reflective cracks allow moisture ingression into the underlying layers, thereby deteriorating the pavement system and resulting in premature failures [28,13]. Furthermore, an increase in vehicular traffic and adverse weather conditions may accelerate the growth of reflective cracks. Consequently, a sustainable solution must be adopted to restore the serviceability and enhance the performance life of asphalt overlays against reflective cracks.

Numerous treatment techniques to restore the serviceability of overlays and resist reflective cracks have been proposed by various researchers [28,41,15,12,17,25] as the outcome of different laboratory and field studies. As a result, geosynthetics in the form of paving fabrics, geogrids and geocomposites have been reported to effectively minimize reflective cracks and enhance the performance life of asphalt overlays substantially [8,22,33,24,40,37]. Moreover, the inclusion of geosynthetics between old and new asphalt layers has led to reductions in the magnitude of permanent deflection of asphalt overlays.

Austin and Gilchrist [5] reported that geogrid reinforcements within

* Corresponding author at: The University of Texas at Austin, 301 E. Dean Keeton St., Room ECJ 9.236, Austin, TX 78712, USA.
E-mail addresses: vinay.vasanth@utexas.edu (V.V. Kumar), sireesh@ce.iith.ac.in (S. Saride), zornberg@mail.utexas.edu (J.G. Zornberg).

https://doi.org/10.1016/j.trgeo.2021.100617
Received 24 February 2021; Received in revised form 23 June 2021; Accepted 5 July 2021
Available online 9 July 2021

Nomenclature

AASHTO	American Association of State Highway and Transportation Officials
ASTM	American Society for Testing and Materials
CBR	California Bearing Ratio
CMD	Cross machine direction
CPD	Cumulative plastic deflection
CPD_{GR}	Cumulative plastic deflection in a geosynthetic-reinforced pavement model
CPD_{UR}	Cumulative plastic deflection in an unreinforced pavement model
EPC	Earth pressure cell
FGC	Fiberglass geogrid composite
GJ	Woven Geo-Jute mat
IRC	Indian Road Congress
LVDT	Linear variable displacement transformer
MD	Machine direction
MORTH	Ministry of Road Transport and Highways
MSA	Million standard axle
N	Number of load cycles
N_{GR}	Number of load cycles sustained by a geosynthetic-reinforced pavement model
N_{UR}	Number of load cycles sustained by an unreinforced pavement model
PET	Polyester
PP	Polypropylene
RDR	Rut depth reduction
SP	Special Publication
TBR	Traffic benefit ratio
UR	Unreinforced
WMM	Wet mix macadam

asphalt layers minimized reflective cracks and reduced surface deflections and the vertical stress acting on the subgrade considerably. Results from beam fatigue tests indicated that the inclusion of geogrids below asphalt overlays decreased reflective cracks by absorbing critical tensile strains at the crack tip and reduced vertical deflections [6,22,39,24]. Large-scale pavement model test results showed an improvement by a factor of 2.5 in reflective crack delay and a roughly 30% to 50% reduction in rut depth in geosynthetic-reinforced models in relation to the rut depth in unreinforced models [34,36,9]. Field investigations of unreinforced and geosynthetic-reinforced asphalt overlays have exhibited reductions in permanent deflection and critical tensile strains in geosynthetic-reinforced sections [26,7,16]. However, these studies have mainly focused on the benefits of geosynthetics used as an anti-reflective cracking system to enhance the performance life of asphalt overlays. More recently, Correia and Zornberg [10], Correia et al. [11] and Lee et al. [27] investigated the structural benefits of asphalt overlays reinforced with geogrids. These studies demonstrated that the presence of geogrids reduce the magnitude of elastic and plastic strains, as well as of vertical and horizontal deflections in asphalt overlays in addition to offer a substantial reduction in reflective cracking. The structural benefits from geosynthetic reinforcements may lead to a reduction in the thickness of asphalt and other pavement layers.

In fact, most of the existing literature regarding geosynthetics in asphalt overlays has focused on their benefits as an anti-reflective cracking system. It is important to note that a small number of researchers have reported the benefits of geosynthetic reinforcements in terms of reduced deflections and critical strains in pavements. Nevertheless, to understand the mechanical response of geosynthetic-reinforced asphalt overlays and evaluate the influence of geosynthetics on the structural benefits of asphalt overlays, full-scale instrumented pavement sections must be tested [32]. The present study evaluates the influence of geosynthetic reinforcements on the structural improvement of asphalt overlays placed on distressed pavement layers using repeated load tests. The performance of unreinforced and geosynthetic-reinforced full-scale instrumented pavement models are evaluated and the structural improvements are quantified in terms of traffic benefit ratio (TBR), rut depth reduction (RDR) and reduction in surface deflection profiles and vertical pressures acting on subgrade.

Materials

Subgrade

The full-scale instrumented pavement models consisted of soil with a California Bearing Ratio (CBR) of 3% to replicate a weak subgrade condition. The particle size distribution curve for the subgrade soil is presented in Fig. 1. The subgrade soil was characterized by a liquid limit of 46%, a plasticity index of 21, and classified as a sandy clay per the Unified Soil Classification System. The maximum dry density and optimum moisture content of the subgrade soil, determined by standard Proctor tests conducted according to ASTM D698 [4], were 1720 kg/m^3 and 15%, respectively.

Base course material

The base course material adopted in this study consisted of Wet Mix Macadam (WMM), which can be used as base/sub-base layers in flexible pavements per India's Ministry of Road Transport and Highways (MORTH) specifications [31]. The particle size distribution of WMM adopted in this study is listed in Table 1. The maximum dry density and optimum moisture content of the WMM, determined by modified Proctor compaction tests conducted according to ASTM D1557 [2], were 2450 kg/m^3 and 6.3%, respectively. The physical properties of the WMM adopted in this study are listed in Table 2.

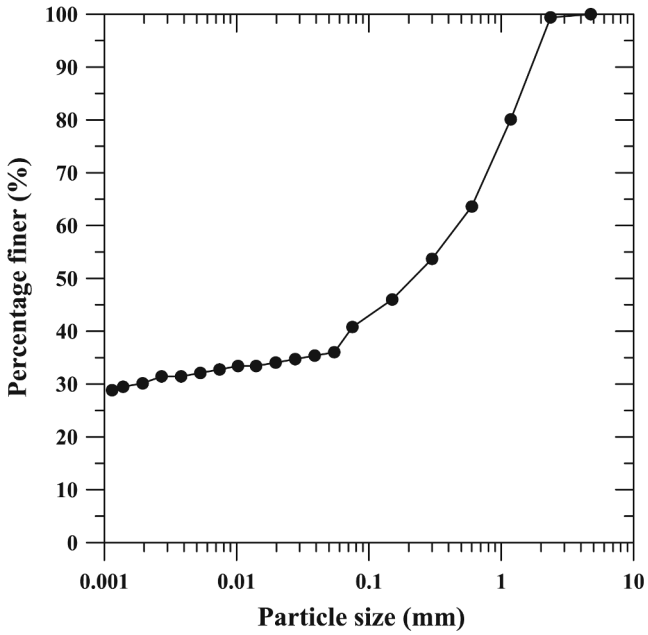

Fig. 1. Grain size distribution curve of the subgrade soil used in the study.

Table 1
Gradation details of Wet Mix Macadam (WMM) material adopted in this study.

Particle size (mm)	Percentage Passing (%)
45	98
22.4	71
11.2	49
4.75	33
2.36	21
0.6	15
0.075	4

Table 2
Properties of Wet Mix Macadam (WMM) material adopted in this study.

S. No.	Property	Standard	Values
1	Aggregate impact value (%)	IS 5640 [21]	25
2	Aggregate crushing value (%)	IS 2386-4 [20]	30
3	Flakiness index (%)	IS 2386-1 [19]	12
4	Elongation index (%)	IS 2386-1 [19]	13

Geosynthetic reinforcements

Four different types of geosynthetic interlayers were selected as asphalt reinforcements for this study based on their physical and mechanical properties: a woven geo-jute mat (GJ); a polypropylene geogrid (PP); a polyester geogrid (PET); and a fiberglass geogrid composite (FGC).

Woven geo-jute mat

The woven Geo-Jute (GJ) mat was manufactured by machine weaving natural jute fibers, as shown in Fig. 2a. The thickness of the GJ was about 1 mm, with an ultimate tensile strength of 25 kN/m at 5% strain and 20 kN/m at 13% strain along the Machine Direction (MD) and Cross-Machine Direction (CMD), respectively.

Polypropylene geogrid

The biaxial Polypropylene (PP) geogrid was manufactured by extending the polypropylene material along the longitudinal (machine) and transversal (cross-machine) directions. The PP geogrid consisted of 40-mm square apertures, had a thickness of 4 mm (Fig. 2b), a rib width of 2 mm, and ultimate tensile strength of 36 kN/m at a strain of 10% and 42 kN/m at a strain of 12% along the MD and CMD, respectively.

Polyester geogrid

The bi-axial Polyester (PET) geogrid was manufactured by knitting together high tenacity polyester yarns. The PET geogrid had square apertures of 18 mm, and rib widths of 3 mm and 4 mm along the MD and CMD, respectively. The PET was fully coated with a polymeric modified binder to enhance its bonding characteristics. The 2-mm thick coated grid (Fig. 2c) had ultimate tensile strength of 48 kN/m at a strain of 18% and 52 kN/m at a strain of 20% along MD and CMD, respectively.

Fiberglass geogrid composite

The Fiberglass Geogrid Composite (FGC) comprised a fiberglass geogrid manufactured by knitting fiberglass filaments and a non-woven geotextile bonded together mechanically, as presented in Fig. 2d. The FGC interlayers had a thickness of 3 mm and an ultimate tensile strength of 28 kN/m at 2% and 25 kN/m at 1.5% along MD and CMD, respectively.

The physical and tensile properties of the geosynthetic-reinforcements adopted in this study are summarized in Table 3.

Binder tack coat and hot mix asphalt

The binder tack coat used in this study was a penetration grade 60/70 bitumen with a penetration value of 66. The properties of the binder tack coat, verified in an experimental testing program, are listed in Table 4. The hot mix asphalt selected for this study was prepared in an asphalt mix plant and transported to the laboratory. The asphalt mix consisted of a penetration grade 60/70 bitumen and aggregates with a particle size distribution as listed in Table 5. Marshall stability tests conducted on the asphalt mix, according to ASTM D6927 [3], determined an optimum binder content of 5.5% by weight of aggregates, and an ultimate strength and flow value of 14.25 kN and 2.5 mm, respectively.

Experimental program

A field performance evaluation of a geosynthetic-reinforced asphalt overlay requires considerable time, materials and cost. These disadvantages were overcome by conducting repeated load tests on the full-scale instrumented pavement models in a controlled laboratory environment at a temperature of 27 ± 1 °C, which also allowed for a fair assessment of their performance. Generally, these performance evaluation studies require a sophisticated loading system, capable of

Table 3
Properties of the geosynthetic reinforcements adopted in this study.

Specifications	woven Geo-Jute mat (GJ)	Polypropylene grid (PP)	Polyester grid (PET)	Fiberglass Geogrid Composite (FGC)
Ultimate tensile strength (kN/m)	25 (MD) 20 (CMD)	36 (MD) 42 (CMD)	48 (MD) 52 (CMD)	28 (MD) 25 (CMD)
Strain at Ultimate tensile strength (%)	5 (MD) 13 (CMD)	10 (MD) 12 (CMD)	18(MD) 20 (CMD)	2 (MD) 1.5 (CMD)
Aperture size (mm × mm)	–	40 × 40	18 × 18	28 × 28

*MD: machine direction; CMD: cross-machine direction.

Fig. 2. Geosynthetic reinforcements used in the study: (a) woven Geo-Jute mat (GJ); (b) Polypropylene geogrid (PP); (c) Polyester geogrid (PET); and (d) Fiberglass Geogrid Composite (FGC).

Table 4
Properties of the binder tack coats adopted in this study.

Serial No.	Properties	Values
1	Penetration (1/10th mm)	66
2	Specific gravity	1.01
3	Viscosity, Brookfield at 60 °C (cP)	460
4	Softening point (°C)	52
5	Ductility (cm)	100+
6	Flash point (°C)	340
7	Fire point (°C)	365

Table 5
Gradation details of aggregates used in the asphalt mix.

Particle size (mm)	Percentage Passing (%)
26.5	100
19	85
13.2	68
9.5	60
4.75	43
2.36	35
1.18	26
0.6	20
0.3	14
0.15	9
0.075	4

replicating real traffic conditions that correspond to Million Standard Axles (MSA) and higher traffic. Details of the full-scale instrumented pavement models and repeated load test procedures are described in the following sections.

Full-scale instrumented pavement model

Five different full-scale instrumented pavement (four geosynthetic-reinforced and one unreinforced) models were designed based on the subgrade CBR value according to Indian Road Congress Special Publication (IRC-SP): 72 (2007) [18]. The full-scale instrumented pavement models were prepared in different stages in an indoor steel tank measuring 1000 mm each in length, width and depth. A schematic representation of a typical cross-section of the geosynthetic-reinforced full-scale instrumented pavement models prepared in this study is presented in Fig. 3. These full-scale instrumented pavement models included a 650-mm-thick weak soil subgrade, a 250-mm-thick base course, a 90-mm-thick distressed asphalt layer, binder tack coat, geosynthetic reinforcements (except the unreinforced model) and a 50-mm-thick hot mix asphalt overlay. Details of full-scale instrumented pavement model preparation are summarized below.

A systematic static compaction procedure was adopted to prepare a weak subgrade (CBR = 3%) that led to the target dry unit weight of 16.8 kN/m^3 and moisture content of 15%. Preliminary trials were initially conducted to determine the number of blows required to achieve the target unit weight and moisture content using a 5-kg static weight compactor with a 500-mm height of fall. Subsequently, 650-mm-thick weak soil subgrade was first compacted in the indoor steel tank in 13 50-mm thick layers. The moisture content was measured at each lift while preparing the test bed and random soil samples were collected and tested after the completion of the test. The uniformity of density and moisture content of the subgrade layers was verified by driving cores at different locations, and the coefficient of variation was quantified as less than 5%. Similar compaction procedures were adopted for chemical stabilization of construction and demolition waste materials by Mohammadinia et al. [29]. The subgrade soil was instrumented with five Earth Pressure Cells (EPC), placed after compaction was completed. The EPCs adopted in the study were manufactured by Tokyo Measuring

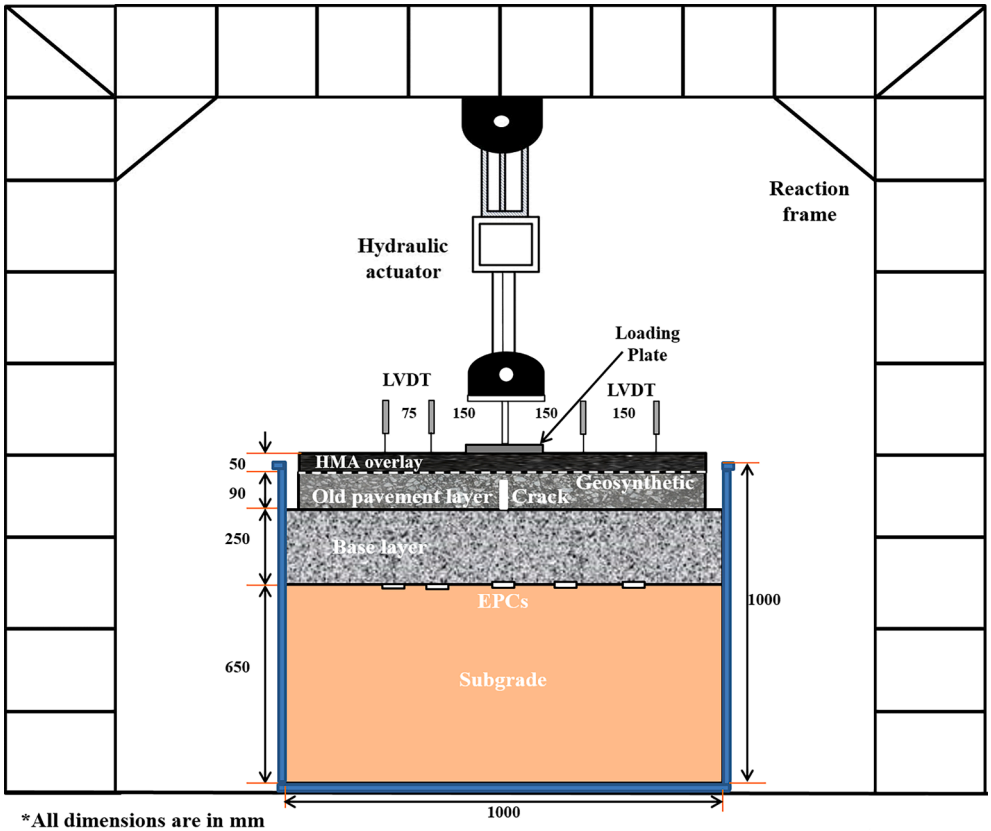

Fig. 3. Schematic of Full-scale Instrumented Pavement model and loading system.

Instruments Laboratory Co. Ltd. (TML, Japan). They had a dual diaphragm structure with 50-mm outside diameter and were capable of measuring dynamic pressures at an output rate of 0.5 mV/V. Circular holes of approximately 50-mm diameter were excavated via trowel, up to a depth of 5 mm, and levelled prior to placement of the EPCs in the holes. Small trenches of approximately 10-mm wide and 10-mm deep were excavated to route the EPC cables to the side of the test tank and then connected to the data loggers installed outside the test tank. The excavated soil was then added back to the holes and trenches, and compacted to achieve the target dry density. Thereafter, a 250-mm-thick WMM base was compacted in five 50-mm-thick layers. The target dry unit weight and water content of the WMM were 23.54 kN/m^3 (96% relative compaction in relation to the modified Proctor compaction) and 6.3%, respectively. Plate vibrators were used to compact the base layer, the density of which was verified after each lift. The compacted WMM surface was allowed to dry completely before applying a prime coat and installing a first fist asphalt layer that corresponds to the old (distressed) pavement, mainly to enhance the bonding between the pavement layers. The distressed asphalt layer was extruded during a highway rehabilitation and cut into dimensions measuring 800 mm in length, 800 mm in width and 90 mm in thickness. Additionally, an 80-mm-deep (90% of layer thickness) and 10-mm-wide notch was cut throughout its entire length to simulate a pre-existing crack in the old asphalt layer. Subsequently, a binder tack coat of penetration grade 60/70 was applied at a residual rate of 0.25 kg/m^2, per MORTH specifications [31]. The geosynthetic reinforcements were then installed (except in unreinforced model) and a 50-mm-thick hot mix asphalt overlay was placed and compacted. Based on the theoretical density of asphalt mix and volume of the layer, the weight of required asphalt mix was calculated and heated in a hot-air oven at 160 °C for about 30 min. Then, the hot mix asphalt was placed and compacted that included vibratory compaction at 40 Hz for 15 min. using a plate vibrator, followed by static compaction using a 5-kg static weight compactor with a square base plate of 200-mm sides having a 500-mm height of fall. Plate vibrator was finally used to level the surface after static compaction and allowed to cure for a day under a room temperature of 27 °C before testing. Four Linear Variable Displacement Transformers (LVDT) manufactured by Tokyo Measuring Instruments Laboratory Co. Ltd. (TML, Japan) were installed on the surface, as shown in Fig. 3, to measure the surface deflection profile of all full-scale models during repeated load tests. As displayed in Fig. 3, the LVDTs were installed on either side of the loading plate at distances of 150 mm, 225 mm and 300 mm from the center of loading plate.

Repeated Load Tests

The repeated load tests were conducted on the full-scale instrumented pavement models prepared in the indoor steel tank (Fig. 3) using a 100-kN capacity servo-hydraulic actuator with a 150-mm dynamic stroke, attached to a 3.5-m-high 200-kN reaction frame. The load was applied through a rigid circular steel plate 15 mm thick and 150 mm in diameter. The test tank and loading plate dimensions were chosen based on observations made in previous studies by Kumar and Saride [23], George et al. [14] and Saride and Kumar [35]. In addition, the boundary effects of rigid test tank on the pavement models were deemed negligible because the distance from the periphery of the loading area to the test tank wall is more than twice the diameter of loading plate [30]. A graphical user-interfaced multipurpose test software was used to develop a typical load pattern that simulates live traffic conditions. The typical load pattern adopted in this investigation is presented in Fig. 4. Maximum and minimum loads of 9.7 kN and 0.97 kN, equivalent to a single axle wheel contact pressure of 550 kPa and 55 kPa, respectively, were applied at a frequency of 1 Hz. Similar contact pressures were adopted by Kumar and Saride [23], Thakur et al. [38], George et al. [14], Mohammadinia et al. [30] and Saride and Kumar [35]. The repeated load tests were carried out up to 100,000 load cycles on all the full-scale models prepared for this study as the corresponding response from the actuator and instrumented sensors was continuously recorded.

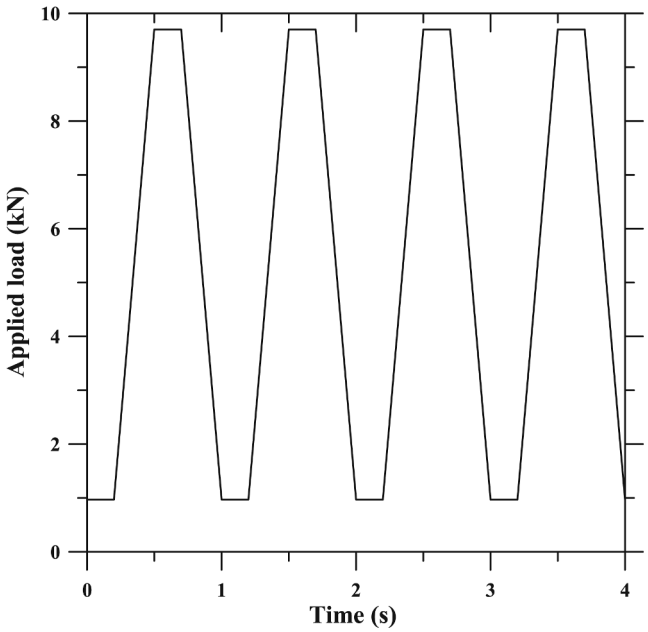

Fig. 4. Typical load pattern adopted in the study.

Results and discussion

Evaluation of load deflection response

The repeated load test was conducted on all the full-scale models in this study to evaluate the influence of geosynthetic reinforcements on the performance of asphalt overlays placed on distressed pavement layers. The repeated load test results (load and displacement measurements from actuator) were processed in the form of time-deflection and pressure-deflection responses. Fig. 5 shows typical results from the unreinforced model. The results in the figure illustrate the increasing deflections with increasing number of load cycles (Fig. 5a) and time (Fig. 5b). The rate of deflection was high initially and decreased as load cycles increased. The deflection for each load cycle was then determined and the total deflection was divided into elastic and plastic deflections, as shown in Fig. 6, for a typical case. The accumulation of plastic deflections under wheel loads leads to the formation of rut. Consequently, the plastic deflection for each load cycle was measured and the Cumulative Plastic Deflections (CPD) were calculated, which represent the rut depth under wheel loads. Similarly, to understand the resilient behavior of the full-scale models under each load cycle, the elastic deflections were calculated and the elastic deflections are shown as a function of number of load cycles in Fig. 7 for the different full-scale instrumented pavement models evaluated in this study. Higher elastic deflections were observed at first due to the high total deflections at that stage and thereafter elastic deflections increased slightly with a subsequent increase in number of load cycles. For instance, elastic deflections in unreinforced model increased from less than 1 mm to 1.3 mm (about 0.3 mm increase) for the initial 10,000 load cycles (see Fig. 7). Instead, the increase in elastic deflections for the next 90,000 load cycles was about 0.08 mm, suggesting a significant decrease in rate of elastic deflections with increasing load cycles. Note that the elastic deflections of the geosynthetic-reinforced models were consistently smaller than those of the unreinforced model, providing evidence of the geosynthetic reinforcement's ability to control elastic deflection. A maximum elastic deflection of 1.38 mm was recorded in the unreinforced model as compared with elastic deflection values of 1.26 mm (GJ), 1.20 mm (PP),

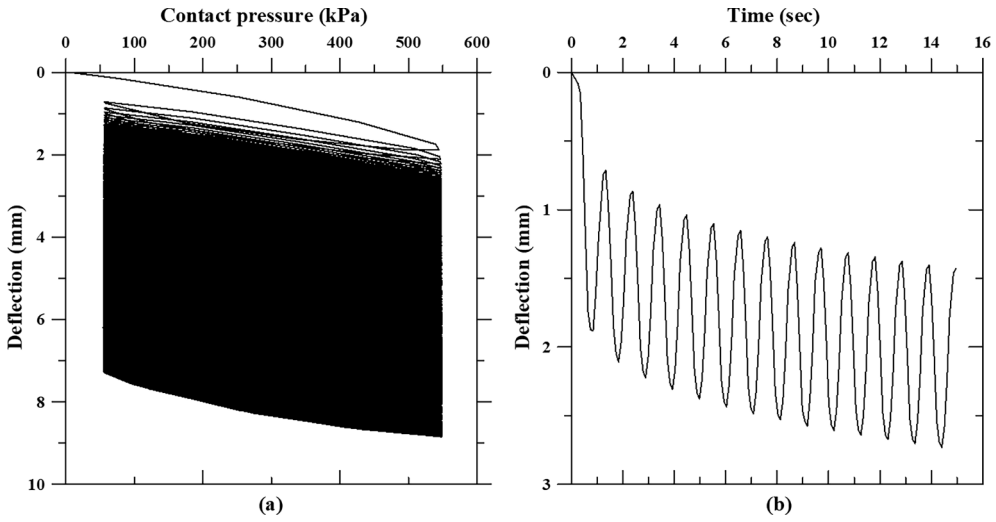

Fig. 5. Unreinforced model test results: (a) typical pressure-deflection plot; and (b) typical time-deflection plot.

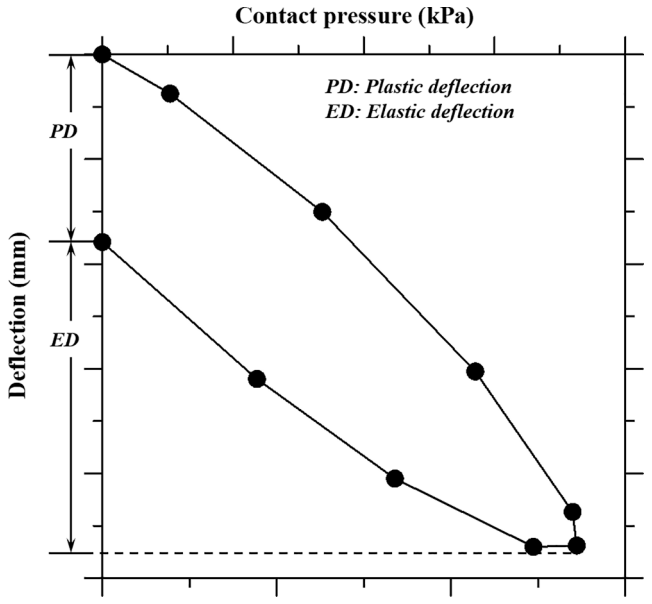

Fig. 6. Elastic and plastic deflections of a typical load cycle.

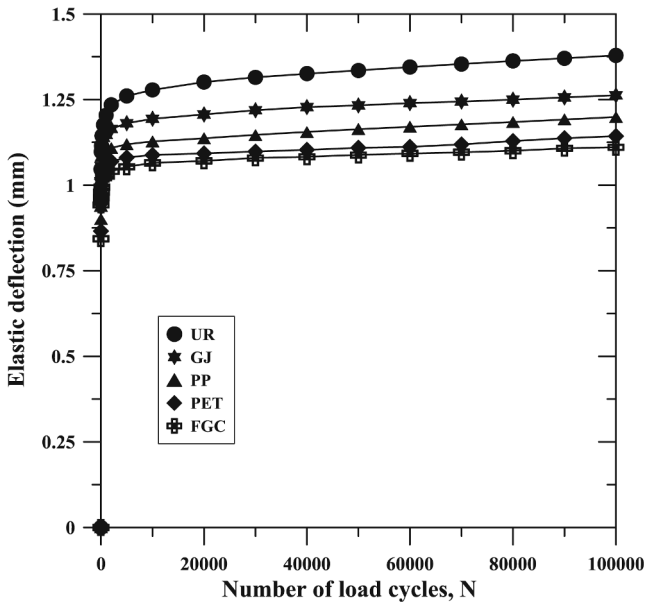

Fig. 7. Elastic Deflection with increasing number of load cycles (N).

1.15 mm (PET), and 1.11 mm (FGC) in the geosynthetic-reinforced models after 100,000 load cycles.

Fig. 8 presents the increasing CPD with number of cycles for all full-scale instrumented pavement models tested in this study. It is evident that the CPD increased with increasing number of load cycles and the CPD in the unreinforced model increased sharply as compared to the CPD in the geosynthetic-reinforced models tested. For instance, after 1000 load cycles, the CPD of the geosynthetic-reinforced models ranged from 2 to 3 mm, while the CPD of the unreinforced model was as high as 4.5 mm. Similarly, following completion of 100,000 load cycles, the CPD of the unreinforced model was 13 mm as opposed to CPD values of 9 mm (GJ), 8 mm (PP), 6.5 mm (PET), and 5.9 mm (FGC) for the geosynthetic-reinforced models. This observation suggests that incorporation of geosynthetic reinforcements below hot mix asphalt overlays improved the structural performance of overlays and restricted permanent deflections substantially. Among the geosynthetic types adopted in this study, the FGC performed comparatively better than the other geosynthetic types, probably due to its ability to induce high tensile unit loads at comparatively low strains (note tensile strength of 28 kN/m at 2% strain in Table 3).

To quantify the structural benefits of the different geosynthetic reinforcements adopted in this investigation, the Traffic Benefit Ratio (TBR), a non-dimensional performance factor was evaluated. The TBR can be defined as the ratio between the number of load cycles required to reach a prescribed permanent deflection in a geosynthetic-reinforced model and such number in an unreinforced model. That is:

$$TBR = \frac{N_{GR}}{N_{UR}} \tag{1}$$

where, N_{GR} and N_{UR} are the number of load cycles in geosynthetic-reinforced and unreinforced models, respectively, to achieve a prescribed CPD.

Fig. 9 presents the relationship between TBR and CPD for all geosynthetic-reinforced models considered in this study. As can be observed in the figure, the TBR increases with increasing CPD. The benefits of incorporating geosynthetic reinforcements below the hot mix asphalt overlay were evident from CPD values as low as 1 mm. For instance, for a CPD of 1 mm, the TBR values obtained for the different geosynthetic-reinforced models were 1.5 (GJ), 1.8 (PP), 2.5 (PET), and 4

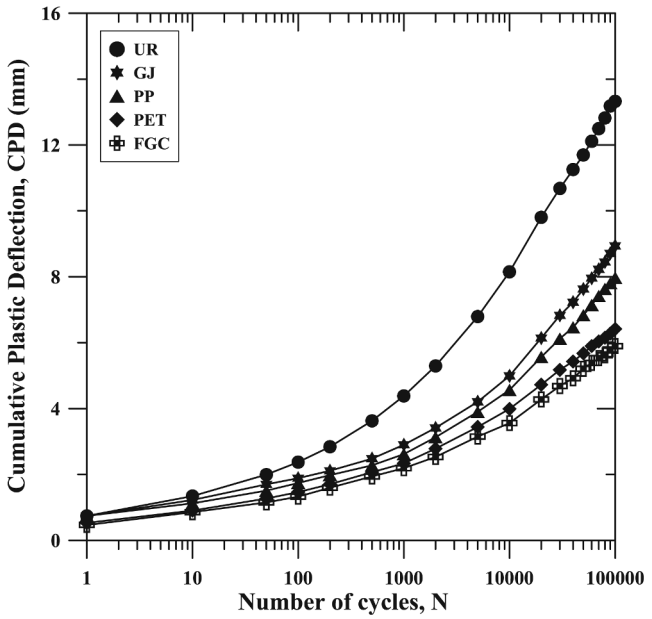

Fig. 8. Cumulative Plastic Deflection (CPD) with increasing number of load cycles.

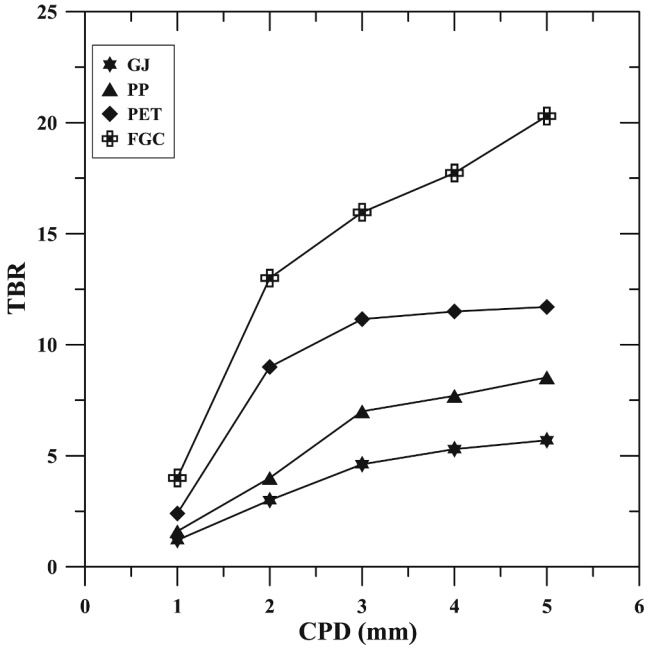

Fig. 9. Relationship between Traffic Benefit Ratio (TBR) and Cumulative Plastic Deflections (CPD) for models using different types of reinforcement.

(FGC). The improvement was observed to increase if the level of performance to quantify the TBR corresponds to comparatively larger CPD values. For example, for a CPD of 3 mm, the TBR values were 4.5 (GJ), 7.5 (PP), 10 (PET), and 16 (FGC) and for a CPD of 5 mm, the TBR was quantified as 5.5 (GJ), 8.5 (PP), 12 (PET), and 20 (FGC) for the geosynthetic-reinforced models.

The overall trend involved a sharp increase in the TBR up to a CPD of approximately 3 mm and a more gradual increase thereafter for all geosynthetic-reinforced models. This trend could be attributed to a comparatively rapid increase in rut depth (quick settlement) of the weak subgrade in the unreinforced model as compared to that in the geosynthetic-reinforced models. It should be noted that TBR data may be adopted in the design of flexible pavements with geosynthetics, according to [1], to optimize the flexible pavement section.

An additional performance indicator, Rut Depth Reduction (RDR), was evaluated to quantify the benefit of incorporating geosynthetic reinforcements in terms of reduction in permanent deflections (rut) under wheel loads. RDR can be defined as the ratio between the difference between the CPD in unreinforced and geosynthetic-reinforced full-scale models and the CPD of the unreinforced model, with the CPD defined for a prescribed number of load cycles. Specifically, RDR can be expressed as:

$$RDR = \left[\frac{CPD_{UR} - CPD_{GR}}{CPD_{UR}}\right] \times 100 \quad (2)$$

where, CPD_{UR} and CPD_{GR} are the cumulative permanent deflections of unreinforced and geosynthetic-reinforced full-scale models, respectively, at a prescribed number of load cycles.

The relationship between RDR and the number of cycles for all the geosynthetic-reinforced models considered in this study can be seen in Fig. 10. The RDR increased significantly with an increase in the number of load cycles (in a log scale), up to 1000 cycles, and continued increasing nominally thereafter. For instance, after 1000 load cycles, the RDR values for the different geosynthetic-reinforced models were approximately 32% (GJ), 37% (PP), 46% (PET), and 52% (FGC). After a 100-fold increase in the number of cycles (i.e. 100,000 load cycles), the RDR values had continued to increase, but a more modest improvement rate, reaching the following values: 37% (GJ), 43% (PP), 51% (PET), and 56% (FGC). These trends substantiate the structural benefits derived from the incorporation of geosynthetic reinforcements under hot mix asphalt overlays.

Table 6 summarizes the repeated load test results for all full-scale instrumented pavement models considered in this study. It is evident that all geosynthetic reinforcements adopted in this study inhibited permanent deflections (rut) under repeated wheel loads effectively and substantially. Among the various geosynthetic-reinforced models tested, the better performance was observed for the FGC-reinforced model, with a TBR of 20 at 5 mm CPD and an RDR of 56% after 100,000 load cycles. It is to be noted that typical geosynthetic interlayers (low tensile strengths) adopted as anti-reflective cracking systems were considered

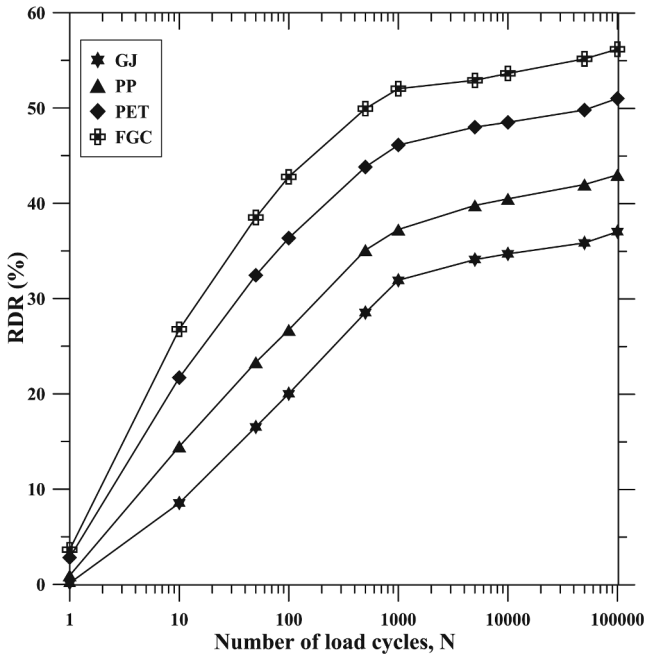

Fig. 10. Increasing Rut Depth Reduction (RDR) with number of load cycles (N) for models using different types of reinforcement.

Table 6
Summary of Repeated Load Test results.

Full-scale Models	CPD (mm) at N = 100,000	TBR at CPD = 5 mm	RDR (%) at N = 100,000
UR	13.32	–	–
GJ	8.94	5.5	37
PP	7.97	8.5	43
PET	6.42	12	51
FGC	5.90	20	56

*CPD: Cumulative permanent deflection; TBR: Traffic benefit ratio; RDR: Rut depth reduction; N: Number of load cycles.

in this study as asphalt reinforcements to evaluate their structural benefits. Hence, it can be summarized that the performance of geosynthetic interlayers as asphalt reinforcements depend on their working tensile and bonding properties with the adjacent asphalt layers, but not on their material composition.

Besides, another important observation displayed that there was no substantial evidence suggesting reflection of the pre-existing crack from old pavement to the overlay in all geosynthetic-reinforced models considered in the study. While, there was a minor hint of reflective cracking witnessed in the overlay of the unreinforced model tested.

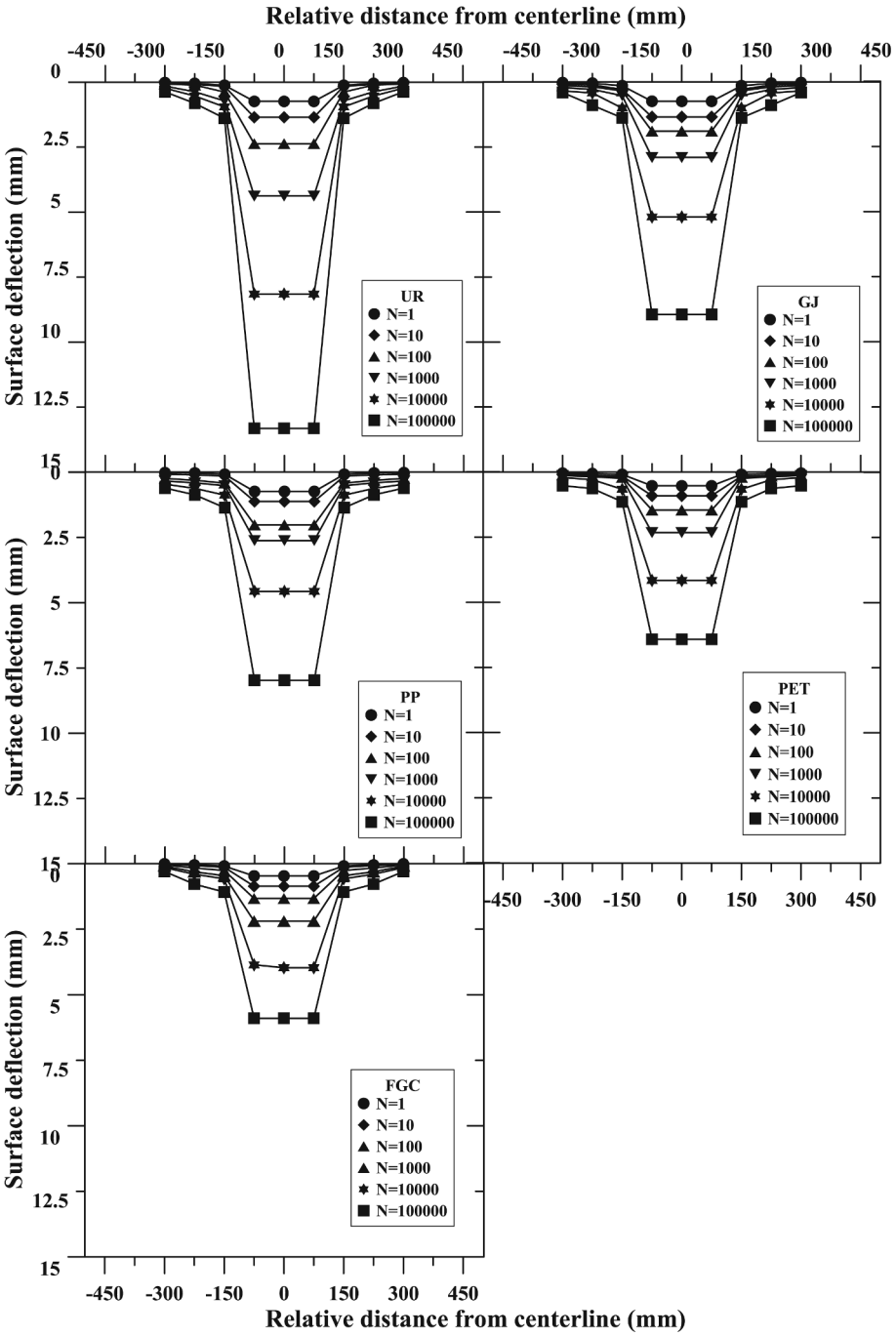

Fig. 11. Surface deflection profile at different load cycles for the full-scale instrumented pavement models: (a) Unreinforced (UR), (b) woven Geo-Jute mat (GJ), (c) Polypropylene geogrid (PP), (d) Polyester geogrid (PET), and (e) Fiberglass Geogrid Composite (FGC).

Evaluation of deflection and contact pressure profiles:

In addition to the information obtained from the load and deflection measurements provided by the actuator, the full-scale models were instrumented with LVDTs and EPCs at the surface and subgrade layers, respectively. These sensors helped define the pavement surface deflection profiles and vertical pressure distribution patterns at the subgrade level under repeated loads.

Profiles of surface deflections on the hot mix asphalt overlay

Surface deflections, recorded by the actuator and LVDTs installed at different locations on the surface of the full-scale instrumented pavement models (Fig. 3), were analyzed to evaluate the surface deflection profiles. Fig. 11 presents the surface deflection profile for all full-scale instrumented pavement models at increasing number of load cycles. It should be noted that higher deflections were recorded directly below the loading region and gradually reduced with increasing distance from the loaded area. For instance, a deflection of 13.3 mm occurred under the load plate and deflections of about 2.5 mm, 1.25 mm and 0.75 mm occurred at radial distances of 150 mm, 225 mm, and 300 mm, respectively, from the center of loading region. This observation is also consistent with that reported in previous literature studies: Siriwardane

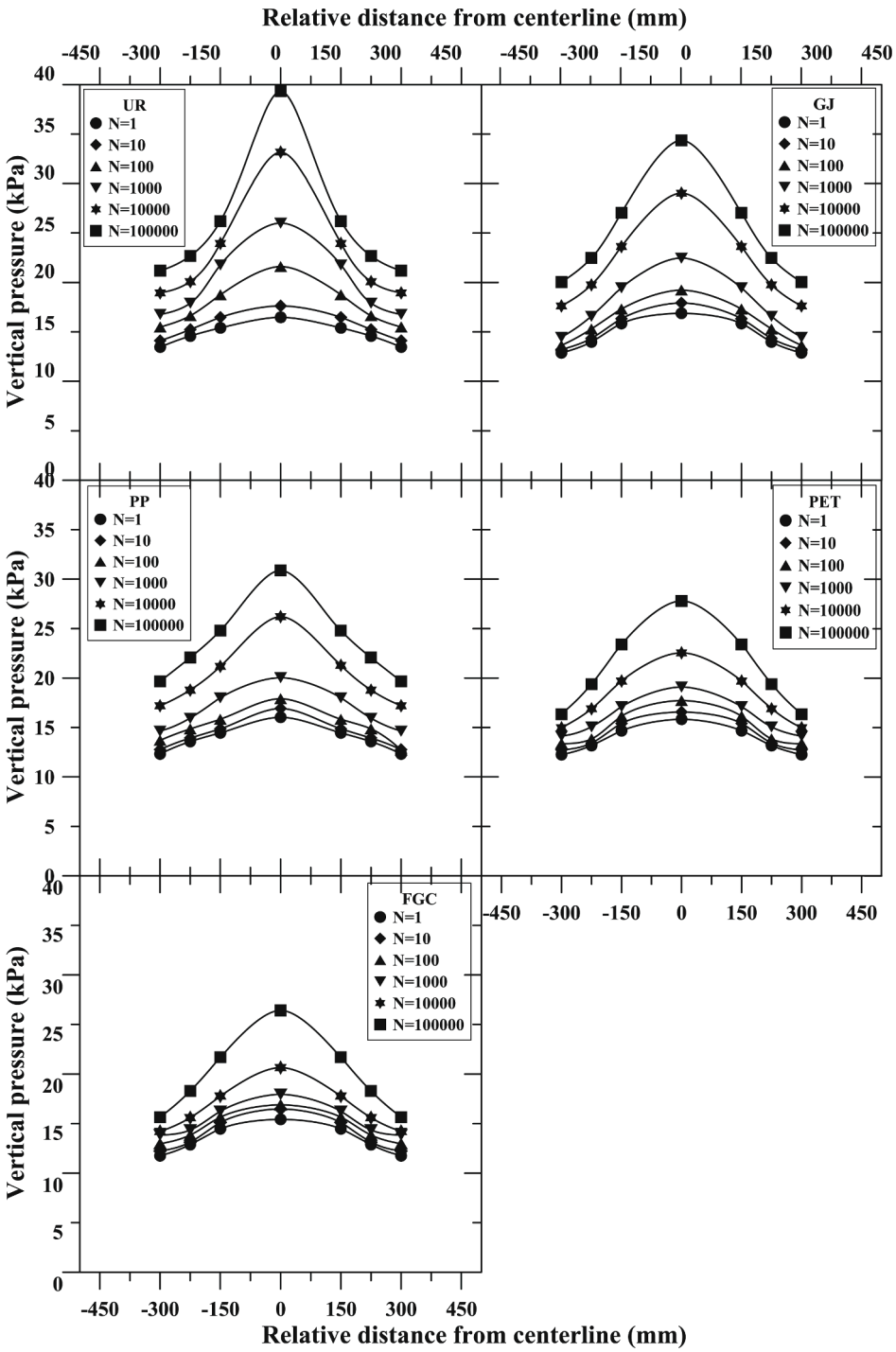

Fig. 12. Vertical pressure on subgrade at different load cycles for all full-scale instrumented pavement models: (a) Unreinforced (UR), (b) woven Geo-Jute mat (GJ), (c) Polypropylene geogrid (PP), (d) Polyester geogrid (PET), and (e) Fiberglass Geogrid Composite (FGC).

et al. [36], Correia and Zornberg [9], Thakur et al. [38], and Correia and Zornberg [10]. As illustrated by the results in Fig. 11, the surface deflection profile of the full-scale instrumented pavement models define a deflection basin that extends below and on either side of the loading region. The results in the figure illustrate the continued deepening of the deflection basin with increasing load cycles. The deflection basins that developed initially (up to approximately 10 load cycles) were reasonably similar for all the full-scale models. Thereafter, the deflection basin of the unreinforced model was consistently deeper than that of the geosynthetic-reinforced models, indicating the triggering of the reinforcing mechanisms in the geosynthetic-reinforced models. Among the geosynthetic-reinforced models, the shallowest deflection basin was observed for the FGC-reinforced model, with a maximum decrease in deflection basin depth of 56% as compared to the unreinforced model, after 100,000 load cycles. Similarly, a decrease in deflection basin depth of 51%, 40%, and 32% was reached for the PET-, PP-, and GJ-reinforced models, respectively, after 100,000 load cycles. The magnitudes of the reductions in deflection basin depth are deemed significant, confirming that the geosynthetic reinforcements embedded below the hot mix asphalt overlay restrict the permanent deflection of the full-scale instrumented pavement models. This is significant, particularly considering that the geosynthetic products evaluated in this study are typically selected to retard reflective cracking rather than to account for an increase in structural capacity. Hence, the variations in the performance of different geosynthetic interlayers may be attributed to their ability to trigger the reinforcement mechanism at low deflections and cogent bonding conditions between the geosynthetic and asphalt layers.

Profiles of contact pressures on the subgrade layer

The distribution of vertical pressures acting on the subgrade layer under different load cycles was measured using five EPCs installed at various locations within the subgrade, as shown in Fig. 3. Fig. 12 depicts the vertical pressure acting on the subgrade under increasing number of load cycles for all full-scale instrumented pavement models. The results are presented in the form of pressure distribution curves. It can be observed that the curvature of the pressure distribution curves for all full-scale instrumented pavement models increases with increasing number of load cycles. The initial response (up to a load cycle of 10) reveals similar pressure distribution curves for all the full-scale models. However, for comparatively higher number of cycles the curvature of the pressure distribution curve for the unreinforced model was consistently higher than that for the geosynthetic-reinforced models. This trend is consistent with the surface deflection profiles shown in Fig. 11, again indicating that triggering of the reinforcing mechanism in the geosynthetic-reinforced models occurs after some initial deflections (or after 10 load cycles in this case). It should also be noted that the pressure distribution curve of the unreinforced model appears sharper, with a peak vertical pressure under the center of the loading plate, while the pressure distribution curves of the geosynthetic-reinforced models appears comparatively flatter. This trend denotes that reinforcing the hot mix asphalt overlay with geosynthetics led to a wider distribution of the contact pressure just under the loaded region, effectively resulting in a decrease in the maximum contact pressure. After 100,000 load cycles, a peak vertical pressure of 39 kPa was recorded over the subgrade of the unreinforced model. In comparison, peak vertical pressures of 35 kPa (GJ), 31 kPa (PP), 28 kPa (PET), and 26 kPa (FGC) were recorded for the geosynthetic-reinforced models, which correspond to reductions in vertical pressure of 10.25% (GJ), 20.51% (PP), 28.20% (PET), and 33.33% (FGC) as compared to the unreinforced model. As stated in the discussion on the surface deflection profile, variations in the performances of the various geosynthetic reinforcements adopted in this study may be attributed to their working tensile and bonding characteristics. For instance, FGC can induce a tensile unit load of 28 kN/m at lower strains on the order of 2%, while PP and PET geogrids induce a comparatively higher tensile unit load of about 40 kN/m to 50 kN/m at higher strains on the order of 12% to 18%. In addition, PP and PET geogrids have open apertures to enhance the bonding characteristics between old and new asphalt layers through confinement, while FGC completely relies on its adhesive ability to asphalt layers.

Overall, it is clear that the adoption of geosynthetic reinforcements embedded below hot mix asphalt overlays controls permanent deflections in roadways effectively and may reduce significantly the vertical pressures acting on the subgrade.

Conclusions

An experimental study on unreinforced and geosynthetic-reinforced full-scale instrumented pavement models was carried out using repeated load test to understand the influence of geosynthetic reinforcements on the structural performance of asphalt overlays placed on distressed pavement layers. The following conclusions can be drawn from the study:

Repeated load test results revealed that all geosynthetic-reinforced models controlled the CPDs consistently better than the unreinforced model. Among them, at least for the geosynthetic products selected in this study, the FGC-reinforced model performed better, with a CPD of 5.90 mm after 100,000 load cycles, followed by the PET (6.42 mm), the PP (7.97 mm), and the GJ (8.94 mm). The CPD of 13.32 mm in the unreinforced model was considerably larger than that in all geosynthetic-reinforced models.

Two performance indicators, TBR and RDR, were evaluated to quantify the structural improvements in the unreinforced and geosynthetic-reinforced models tested. The FGC-reinforced model achieved a TBR of 20 at a CPD of 5 mm, followed by TBR values of 12 (PET), 8.5 (PP), and 5.5 (GJ). A maximum RDR of 56% was observed in the FGC-reinforced model followed by RDR values of 51% (PET), 43% (PP), and 37% (GJ) after 100,000 load cycles.

Data obtained from the LVDTs installed on the surface layer of the full-scale instrumented pavement models tested under repeated loads revealed maximum deflections below the loading plate that decreased as distance from loading plate increased. All geosynthetic-reinforced models resisted surface deflections effectively, with reduced deflection basins on the order of 56% (FGC), 51% (PET), 43% (PP), and 37% (GJ) as compared with the unreinforced model, after 100,000 load cycles.

Data obtained from the EPCs installed at the subgrade level of the full-scale instrumented pavement models tested under repeated loads revealed that all geosynthetic reinforcements reduced the peak vertical pressure distribution on the subgrade under the loading plate by distributing them to a wider area, as compared to the unreinforced model. Reductions in the peak vertical pressure distribution on the subgrade were approximately 33.33% (FGC), 28.20% (PET), 20.51% (PP), and 10.25% (GJ) in the geosynthetic-reinforced models, as compared to the unreinforced model, after 100,000 load cycles.

Overall, it is evident that the geosynthetic reinforcements embedded below the hot mix asphalt overlays in this study restricted permanent deflections and reduced the vertical pressure distribution on the subgrade under repeated wheel loads successfully. However, the extent of the structural benefit depends on the working mechanical and tensile properties of the geosynthetic reinforcements adopted in the study.

Funding

This research did not receive any specific grant from funding agencies in the public, commercial, or not-for-profit sectors.

CRediT authorship contribution statement

V. Vinay Kumar: Conceptualization, Data curation, Formal analysis, Investigation, Methodology, Validation, Visualization, Writing - original draft. **Sireesh Saride:** Conceptualization, Methodology, Resources, Supervision, Visualization, Writing - review & editing. **Jorge G. Zornberg:** Supervision, Visualization, Writing - review & editing.

Declaration of Competing Interest

The authors declare that they have no known competing financial interests or personal relationships that could have appeared to influence the work reported in this paper.

References

[1] AASHTO R 50. (2009). Recommended Practice for Geosynthetic Reinforcement of the Aggregate Base Course of Flexible Pavement Structures. Standard by American Association of State and Highway Transportation Officials, 2009.

[2] ASTM D1557. Standard Test Methods for Laboratory Compaction Characteristics of Soil Using Modified Effort. Annual Book of ASTM Standards, ASTM International, West Conshohocken, PA.

[3] ASTM D6927. Standard Test Method for Marshall Stability and Flow of Asphalt Mixtures. Annual Book of ASTM Standards, ASTM International, West Conshohocken, PA.

[4] ASTM D698. Standard Test Methods for Laboratory Compaction Characteristics of Soil Using Standard Effort. Annual Book of ASTM Standards, ASTM International, West Conshohocken, PA.

[5] Austin RA, Gilchrist AJT. Enhanced performance of asphalt pavements using geocomposites. Geotext Geomembr 1996;14:175–86.

[6] Brown SF, Thom NH, Sanders PJ. A study of grid reinforced asphalt to combat reflection cracking. J Assoc Asphalt Paving Technolog 2001;70:543–69.

[7] Buhler, A. Study the Effect of Grid Reinforcement in Pavement Restoration, PhD Thesis, Submitted to ITA, Sao Jose dos Campos, Sao Paulo, Brazil, 2007.

[8] Cleveland GS, Button JW, Lytton RL. *Geosynthetic in Flexible and Rigid Pavement Overlay*, Texas Transportation Institute. Texas A&M University System. Report. 2002:1777–81.

[9] Correia NS, Zornberg JG. Mechanical response of flexible pavements enhanced with geogrid-reinforced asphalt overlays. Geosynthetics Int 2016;23(3):183–93.

[10] Correia NS, Zornberg JG. Strain distribution along geogrid-reinforced asphalt overlays under traffic loading. Geotext Geomembr 2018;46:111–20.

[11] Correia NS, Esquivel ER, Zornberg JG. Mechanical response of flexible pavements enhanced with geogrid-reinforced asphalt overlays. J Transport Eng, Part B: Pavem, ASCE 2018;144(2):04018020.

[12] Dhakal N, Elseifi MA, Zhang Z. Mitigation strategies for reflection cracking in rehabilitated pavements - A synthesis. Int J Pavem Res Technol 2016;9(3):228–39.

[13] Elseifi MA, Al-Qadi IL. A simplified overlay design model against reflective cracking utilizing service life prediction. Road Mater Pavem Design 2004;5(2):169–91.

[14] George AM, Banerjee A, Puppala AJ, Saladhi M. Performance evaluation of geocell-reinforced reclaimed asphalt pavement (RAP) bases in flexible pavements. Int J Pavem Eng 2019;22(2):181–91. https://doi.org/10.1080/10298436.2019.1587437.

[15] Gonzalez-Torre I, Calzada-Peres MA, Vega-Zamanillo A, Castro-Fresno D. Experimental study of the behavior of different geosynthetics as anti-reflective cracking systems using a combined-load fatigue test. Geotext Geomembr 2015;43(4):345–50.

[16] Graziani A, Pasquini E, Ferrotti G, Virgili A, Canestrari F. Structural response of grid-reinforced bituminous pavements. Mater Struct 2014;47(8):1391–408.

[17] Habbouche J, Hajj E, Morian NE, Sebaaly PE, Piratheepan M. Reflective cracking relief interlayer for asphalt pavement rehabilitation: from development to demonstration. Road Mater Pavem Design 2017;18(sup4):30–57.

[18] IRC: SP-72. (2007). Guidelines for the Design of Flexible Pavements for Low Volume Rural Roads. Indian Road Congress (IRC), New Delhi.

[19] IS 2386-1. Methods of Test for Aggregates for Concrete. Part 1. Determination of Particle size and shape, Bureau of Indian Standards, Manak Bhavan, New Delhi.

[20] IS 2386-4. Methods of Test for Aggregates for Concrete. Part 4. Determination of Mechanical properties, Bureau of Indian Standards, Manak Bhavan, New Delhi.

[21] IS 5640. Method of Testing for determining Aggregates Impact Value of soft coarse aggregates, Bureau of Indian Standards, Manak Bhavan, New Delhi.

[22] Khodaii A, Fallah S, Nejad FM. Effects of Geosynthetics on Reduction of Reflection Cracking in Asphalt Overlay. Geotext Geomembr 2009;27:131–40.

[23] Kumar VV, Saride S. Rutting Behavior of Geocell Reinforced Base Layer Overlying Weak Sand Subgrades. Procedia Eng 2016;143:1409–16.

[24] Kumar VV, Saride S. Use of Digital Image Correlation for the Evaluation of Flexural Fatigue Behavior of Asphalt Beams with Geosynthetic Interlayers. Transport Res Record: J Transport Res Board 2017;2631:55–64.

[25] Kumar VV, Saride S. Evaluation of cracking resistance potential of geosynthetic-reinforced asphalt overlays using direct tensile strength tests. Constr Build Mater 2018;162:37–47.

[26] Laurinavicius A, Oginskas R. Experimental research on the development of rutting in asphalt concrete pavements reinforced with geosynthetic materials. J Civil Eng Manage 2006;12(4):311–7.

[27] Lee J-H, Baek S-B, Lee K-H, Kin J-S, Jeong J-H. Long-term performance of fiber-grid-reinforced asphalt overlay pavements: A case study of Korean national highways. J Traffic Transport Eng 2019;6(4):366–82.

[28] Lytton RL. Use of geotextiles for reinforcement and strain relief in asphalt concrete. Geotext Geomembr 1989;8(3):217–37.

[29] Mohammadinia A, Arulrajah A, Horpibulsuk S, Shourijeh PT. Impact of potassium cations on the light chemical stabilization of construction and demolition wastes. Constr Build Mater 2019;203:69–74.

[30] Mohammadinia A, Arulrajah A, Disfani MM, Darmawan S. Small-strain behavior of cement-stabilized recycled concrete aggregate in pavement base layers. J Mater Civ Eng, ASCE 2019;31(5):04019044.

[31] MORTH. Specifications for Road and Bridge Works. Indian Road Congress (IRC), New Delhi: Ministry of Road Transport and Highways; 2013.

[32] Perkins SW. Mechanical response of geosynthetic reinforced flexible pavements. Geosynthetics Int 1999;4(6):347–82.

[33] Safavizadeh SA, Wargo A, Guddati M, Kim YR. Investigating Reflective Cracking Mechanisms in Grid-Reinforced Asphalt Specimens. Transport Res Record: J Transport Res Board 2015;2507:29–38.

[34] Sanders PJ. Reinforced Asphalt Overlays for Pavements. PhD Thesis, submitted to. UK: University of Nottingham; 2001.

[35] Saride S, Kumar VV. Estimation of Service life of Geosynthetic-Reinforced Asphalt Overlays from Beam and Large-Scale Fatigue Tests. J Test Eval 2019;47(4):2693–716.

[36] Siriwardane H, Gondle R, Bora K. Analysis of flexible pavements reinforced with geogrids. Geotech Geol Eng 2010;28(3):287–97.

[37] Sudarsanan N, Arulrajah A, Karpurapu R, Amrithalingam V. Fatigue performance of geosynthetic reinforced asphalt concrete beams. J Mater Civ Eng, ASCE 2020;32(8).

[38] Thakur JK, Han J, Parsons R. Factors Influencing Deformations of Geocell-Reinforced Recycled Asphalt Pavement Bases under Cyclic Loading. J. Mater. Civ. Eng., ASCE 2017;29(3):04016240.

[39] Virgili A, Canestrari F, Grilli A, Santagata FA. Repeated load test on bituminous systems reinforced by geosynthetics. Geotext Geomembr 2009;27:187–95.

[40] Wargo A, Safavizadeh SA, Kim YR. Comparing the Performance of Fiberglass Grid with Composite Interlayer Systems in Asphalt Concrete. Transport Res Rec: J Transport Res Board 2017;2631:123–32.

[41] Zamora-Barraza D, Calzada-Peres MA, Castro-Fresno D, Vega-Zamanillo A. Evaluation of anti-reflective cracking systems using geosynthetics in the interlayer zone. Geotext Geomembr 2011;29(2):130–6.